Hindawi
Advances in Mathematical Physics
Volume 2021, Article ID 6664039, 15 pages
https://doi.org/10.1155/2021/6664039

*Research Article*

# Line Soliton Interactions for Shallow Ocean Waves and Novel Solutions with Peakon, Ring, Conical, Columnar, and Lump Structures Based on Fractional KP Equation

**Bo Xu,[1,2] Yufeng Zhang,[1] and Sheng Zhang[3]**

[1]*School of Mathematics, China University of Mining and Technology, Xuzhou 221116, China*
[2]*School of Educational Sciences, Bohai University, Jinzhou 121013, China*
[3]*School of Mathematical Sciences, Bohai University, Jinzhou 121013, China*

Correspondence should be addressed to Yufeng Zhang; zyfxz@cumt.edu.cn and Sheng Zhang; szhangchina@126.com

Received 4 December 2020; Revised 31 January 2021; Accepted 3 February 2021; Published 27 February 2021

Academic Editor: Ming Mei



It is well known that the celebrated Kadomtsev-Petviashvili (KP) equation has many important applications. The aim of this article is to use fractional KP equation to not only simulate shallow ocean waves but also construct novel spatial structures. Firstly, the definitions of the conformable fractional partial derivatives and integrals together with a physical interpretation are introduced and then a fractional integrable KP equation consisting of fractional KPI and KPII equations is derived. Secondly, a formula for the fractional $n$-soliton solutions of the derived fractional KP equation is obtained and fractional line one-solitons with bend, wavelet peaks, and peakon are constructed. Thirdly, fractional X-, Y- and 3-in-2-out-type interactions in the fractional line two- and three-soliton solutions of the fractional KPII equation are simulated for shallow ocean waves. Besides, a falling and spreading process of a columnar structure in the fractional line two-soliton solution is also simulated. Finally, a fractional rational solution of the fractional KP equation is obtained including the lump solution as a special case. With the development of time, the nonlinear dynamic evolution of the fractional lump solution of the fractional KPI equation can change from ring and conical structures to lump structure.

## 1. Introduction

As Ablowitz and Baldwin [1] pointed, the two-space and one-time dimensional equation governing unidirectional, maximally balanced, weakly nonlinear shallow water waves with weak transverse variation is the celebrated KP equation [2]:

$$\frac{\partial}{\partial x}\left(\frac{1}{\sqrt{gh}}\eta_t+\eta_x+\frac{3}{2h}\eta\eta_x+\frac{h^2\gamma}{2}\eta_{xxx}\right)+\frac{1}{2}\eta_{yy}=0, \quad (1)$$

where $g$ is gravity, $h$ is constant mean height, $\eta=\eta(x,y,t)$ is wave high above $h$, $\gamma=1-\tau/3$, $\tau=T/(\rho g h^2)$ is dimensionless surface tension coefficient, and $\rho$ is density. Obviously, if $\eta$ is not related to $y$, then Equation (1) reduces to the Korteweg-de Vries (KdV) equation [3]. So, KP Equation (1) can be regarded as an extension of the KdV equation to two-dimensional space. In nondimensional form, KP Equation (1) can be rescaled as [1]:

$$\left(u_t+6uu_x+u_{xxx}\right)_x+3\sigma u_{yy}=0, \quad (2)$$

where $\sigma=1$ and $\sigma=-1$, depending on the sign of $\gamma$, correspond to KPII and KPI equations, respectively. The KPI equation exists lump solutions rationally localized in all directions in the space, for example, those [4] obtained by Ma. At the same time, $n$-soliton solutions with a single phase, called line solitons, have been found for the KPII equation by the Hirota bilinear method [5].

Recently, Abolwitz and Baldwin [1] obtained line two- and three-soliton solutions with X-, Y-, and more complex-type interactions of the KPII equation. Interestingly, such types of X, Y, and more complex (for example 3-in-2-out) interactions have been observed to appear frequently in

shallow water on two relatively flat beaches. Three types (short stem, long stem with lower and higher incoming line solitons) of X- and typical Y-type ocean wave interactions observed by Abolwitz and Baldwin in Mexico and California occur daily, shortly before and after low tide. However, these complex interactions like the 3-in-2-out one with three incoming line solitons on one side and two outgoing line solitons on the other side are much less frequent than X- and Y-type interactions. If the distances in the open-ocean direction are large enough, the destructive tsunami waves can merge in similar ways to the initial formation of an X- or Y-type wave, such as the observations that happen in the tsunami induced by the 2011 Japanese Tohoku-Oki earthquake indicating there was a merging phenomenon from a cylindrical-wave-type interaction. For more details, refer to Ref. [1].

The aim of this article is to derive not only the X-, Y-, and 3-in-2-out-type interactions but also other novel solutions forming ring, conical, columnar, and lump structures from a fractional version of KP Equation (2):

$$\left(u_{t,c}^{(\alpha)}+6uu_{x,a}^{(\alpha)}+u_{x,a}^{(3\alpha)}\right)_{x,a}^{(\alpha)}+3\sigma u_{y,b}^{(2\alpha)}=0,\quad 0<\alpha=\frac{p}{q}\le 1,\sigma=\pm 1, \tag{3}$$

with the conformable fractional partial derivatives $D_{x,a}^{\alpha}$, $D_{y,b}^{\alpha}$, and $D_{t,c}^{\alpha}$ (see the next section for Definitions 1 and 2). Some novel spatial structures obtained in fractional KP Equation (3) cannot be derived from corresponding integral-order KP Equation (2). This is due to the irreplaceable role of fractional calculus [6–23].

The rest of this paper is organized as follows. In Section 2, we present the conformable fractional partial derivatives and integrals and give a physical interpretation of the conformable fractional derivative. In Section 3, we derive fractional KP Equation (3) from the corresponding fractional Lax pair. In Section 4, we transform fractional KP Equation (3) into bilinear form and then not only construct its fractional line solitons with X-, Y-, and 3-in-2-out interactions but also simulate a falling and spreading process of a columnar structure in the fractional KPII equation. At the same time, we construct a fractional rational solution of fractional KP Equation (3) and employ it to form ring, conical, and lump structures of the fractional KPI equation. In Section 5, we conclude this paper.

## 2. Definitions and Physical Interpretation

We give, in this section, the definitions of the conformable fractional partial derivatives and integrals. Since these definitions are based on the similar definitions in Ref. [24], we add this reference when defining them.

*Definition 1* [24]. For the given function $u(x,t)$: $\mathrm{R}\times\mathrm{R}\longrightarrow\mathrm{C}$, arbitrary constant $a\in\mathrm{R}$, and fractional-order $\alpha\in(0,1]$, the conformable fractional partial derivative with respect to $x$ has the definition:

$$D_{x,a}^{\alpha}u(x,t)=u_{x,a}^{(\alpha)}(x,t)=\lim_{\varepsilon\to 0}\frac{u\left[x+\varepsilon(x-a)^{1-\alpha},t\right]-u(x,t)}{\varepsilon},\quad 0<\alpha=\frac{p}{q}\le 1, \tag{4}$$

where $p$ and $q$ are coprime and positive integers guaranteeing $(x-a)^{\alpha}$ can return a unique real or complex value. Here, if $q$ is an even number, then $(x-a)^{\alpha}$ is stipulated to locate in the first quadrant of the complex plane and has the smallest imaginary part for arbitrary $x<a$. Note that $u_{x,a}^{(\alpha)}(x,t)|_{x=a}=\lim_{x\to a^{+}}u_{x,a}^{(\alpha)}(x,t)$ is a supplement of Definition 1. As a special case of Definition 1, we have the following Definition 2.

*Definition 2* [24]. If function $u(x,t)$: $\mathrm{R}\times\mathrm{R}\longrightarrow\mathrm{R}$, arbitrary constant $a\in\mathrm{R}$, and fractional-order $\alpha\in(0,1]$ are given, then we define the conformable fractional partial derivative with respect to $x$:

$$D_{x,a}^{\alpha}u(x,t)=u_{x,a}^{(\alpha)}(x,t)=\lim_{\varepsilon\to 0}\frac{u\left\{x+\varepsilon\left[(x-a)^{p}\right]^{1/p-1/q},t\right\}-u(x,t)}{\varepsilon},\quad 0<\alpha=\frac{p}{q}\le 1, \tag{5}$$

where $p$ and $q$ are coprime and positive integers, and $p$ is an even number. A supplement of Definition 2 is the stipulation $u_{x,a}^{(\alpha)}(x,t)|_{x=a}=\lim_{x\to a^{+}}u_{x,a}^{(\alpha)}(x,t)$.

*Definition 3* [24]. The conformable fractional integral of function $u(x,t)$: $\mathrm{R}\times\mathrm{R}\longrightarrow\mathrm{C}$ is defined:

$$I_{x,a}^{\alpha}u(x,t)=\partial_{x,a}^{-\alpha}u(x,t)=\int_{a}^{x}(x-a)^{1-\alpha}u(x,t)\,dx,\quad 0<\alpha=\frac{p}{q}\le 1, \tag{6}$$

where $a\in\mathrm{R}$ is an arbitrary constant, and $(x-a)^{\alpha}$ is stipulated to return a unique real or complex value.

*Definition 4* [24]. Suppose that $p$ is an even number and $a\in\mathrm{R}$ is an arbitrary constant, the conformable fractional integral of function $u(x,t)$: $\mathrm{R}\times\mathrm{R}\longrightarrow\mathrm{R}$ is defined:

$$I_{x,a}^{\alpha}u(x,t)=\partial_{x,a}^{-\alpha}u(x,t)=\int_{a}^{x}\left[(x-a)^{p}\right]^{1/p-1/q}u(x,t)\,dx,\quad 0<\alpha=\frac{p}{q}\le 1. \tag{7}$$

We may say $u(x,t)$ is $\alpha$-differentiable with respect to $x$ in the case that Equation (4) or (5) holds. By comparisons, we can see that Definitions 1–4 include those in [24, 25] as special cases. The defined conformable partial derivatives and integrals in Definitions 1–4 have some basic properties, which are all similar to the ones in [24, 25]. Only one of them is listed here, and the rest are omitted, that is, $D_{x,a}^{\alpha}u(x,t)=(x-a)^{1-\alpha}u_{x}(x,t)$. In other words, $D_{x,a}^{\alpha}u(x,t)$ is the product of the rate of change of $u(x,t)$ along the $x$-axis and $(x-a)^{1-\alpha}$, which is helpful to understand the physical meaning of conformable fractional partial derivatives.

It is a challenging problem to explore the physical or geometric meaning of fractional derivatives and integrals. As Xue [26] pointed out, although fractional calculus was born more than 300 years ago, there are no widely accepted physical and geometric interpretations of fractional derivatives and fractional integrals. Inspired by Podlubny's work [27], we would like to give a physical explanation of the conformable fractional derivative $T_\alpha(f)(t)$ [25]. Suppose an object moves with variable acceleration, and its variable acceleration and velocity are $a(t)$ and $v(t)$ at time $t$, respectively. Furthermore, it is assumed that the relationship between the cosmic time [27] (real time) $T = g_t(\tau)$ and the individual time [27] (inaccurate timing) $\tau$ satisfies

$$g_t(\tau) = \frac{t^{2-\alpha} + \tau^{2-\alpha} - t}{2-\alpha}. \tag{8}$$

With the above preparation, we can see that the real velocity $v_O(t)$ of the moving object with the variable acceleration $a(\tau)$ in the individual time measure at cosmic time $T$ is

$$v_O(t) = \int_0^t a(\tau)\mathrm{d}g_t(\tau) = \int_0^t v'(\tau)\tau^{1-\alpha}\mathrm{d}\tau, \tag{9}$$

from which the variable acceleration $a_O(t)$ at time $t$ can be derived as the following:

$$a_O(t) = v'_O(t) = \frac{d}{dt}\int_0^t v'(\tau)\tau^{1-\alpha}d\tau = v'(t)t^{1-\alpha} = T_\alpha(v)(t). \tag{10}$$

Therefore, the $\alpha$-order conformable fractional derivative $T_\alpha(v)(t)$ of the velocity function $v(t)$ is just the variable acceleration $a_O(t)$ from the observer's perspective with accurate time. This is a physical interpretation of the conformable fractional derivative. For the special case $\alpha = 1$, Equations (8) and (10) reduce $g_t(\tau) = \tau$ and $a_O(t) = v'(t) = a(t)$, respectively. That is to say, when there is no difference between the cosmic time and the individual time, the corresponding variable accelerations are equal.

## 3. Lax Representation

For the Lax representation of fractional KP Equation (3), we have the following Theorem 5.

**Theorem 5.** *Fractional KP Equation (3) is the Lax integrable, the Lax representation of which is*

$$\left[L, A - \partial^\alpha_{t,c}\right] = 0, \tag{11}$$

*with the Lax pair*

$$\begin{aligned} L &= \sqrt{\sigma}\partial^\alpha_{y,b} + \partial^{2\alpha}_{x,a} + u, \\ A &= -4\partial^{3\alpha}_{x,a} - 6u\partial^\alpha_{x,a} - 3u^{(\alpha)}_{x,a} + 3\sqrt{\sigma}\partial^{-\alpha}_{x,a}u^{(\alpha)}_{y,b}. \end{aligned} \tag{12}$$

*Proof.* It is easy to derive that

$$\begin{aligned} LA = {} & -4\partial^{5\alpha}_{x,a} - 6u\partial^{3\alpha}_{x,a} - 3u^{(\alpha)}_{x,a}\partial^{2\alpha}_{x,a} - u\left(4\partial^{3\alpha}_{x,a} + 6u\partial^\alpha_{x,a} + 3u^{(\alpha)}_{x,a}\right) \\ & - 12u^{(\alpha)}_{x,a}\partial^{2\alpha}_{x,a} - 12u^{(2\alpha)}_{x,a}\partial^\alpha_{x,a} - 3u^{(3\alpha)}_{x,a} \\ & + \sqrt{\sigma}\left(-4u^{(3\alpha)}_{x,a} - 6u\partial^\alpha_{x,a} - 3u^{(\alpha)}_{x,a} + 3\sqrt{\sigma}\partial^{-\alpha}_{x,a}u^{(\alpha)}_{y,b}\right)\partial^\alpha_{y,b} \\ & + 3\sqrt{\sigma}\left(\partial^{-\alpha}_{x,a}u^{(\alpha)}_{y,b}\right)\left(\partial^{2\alpha}_{x,a} + u\right) + 3\sigma\partial^{-\alpha}_{x,a}u^{(2\alpha)}_{y,b}, \end{aligned} \tag{13}$$

$$\begin{aligned} AL = {} & -4\partial^{5\alpha}_{x,a} - 6u\partial^{3\alpha}_{x,a} - 3u^{(\alpha)}_{x,a}\partial^{2\alpha}_{x,a} - u\left(4\partial^{3\alpha}_{x,a} + 6u\partial^\alpha_{x,a} + 3u^{(\alpha)}_{x,a}\right) \\ & - 12u^{(\alpha)}_{x,a}\partial^{2\alpha}_{x,a} - 12u^{(2\alpha)}_{x,a}\partial^\alpha_{x,a} - 4u^{(3\alpha)}_{x,a} - 6uu^{(\alpha)}_{x,a} \\ & + \sqrt{\sigma}\left(-4\partial^{3\alpha}_{x,a} - 6u\partial^\alpha_{x,a} - 3u^{(\alpha)}_{x,a} + 3\sqrt{\sigma}\partial^{-\alpha}_{x,a}u^{(\alpha)}_{y,b}\right)\partial^\alpha_{y,b} \\ & + 3\sqrt{\sigma}\left(\partial^{-\alpha}_{x,a}u^{(\alpha)}_{y,a}\right)\left(\partial^{2\alpha}_{x,a} + u\right). \end{aligned} \tag{14}$$

On the other hand, we can verify the relation:

$$\left[L, -D^\alpha_{t,c}\right] = u^{(\alpha)}_{t,c}. \tag{15}$$

Substituting Equations (13) and (14) into Equation (11) yields

$$u^{(\alpha)}_{t,c} + 6uu^{(\alpha)}_{x,a} + u^{(3\alpha)}_{x,a} + 3\sigma\partial^{-\alpha}_{x,a}u^{(2\alpha)}_{y,b} = 0. \tag{16}$$

Further taking $\alpha$-order conformable partial derivative with respect to $x$, we finally transform Equation (16) into Equation (3). Thus, we complete the proof.

## 4. Fractional Line Soliton Solutions and Their Interactions

There are four parts in this section for the fractional line soliton solutions and their interactions of fractional KP Equation (3): one part is the bilinearization of Equation (3), and the other three parts are the simulations for X-, Y-, and 3-in-2-out-type interactions and peakon, ring, conical, columnar, and lump structures in the obtained fractional line one-, two-, and three-soliton solutions.

*4.1. Bilinearization and Formula of Soliton Solutions.* We have the following Theorem 6 for the bilinear form of fractional KP Equation (3).

**Theorem 6.** *Let*

$$u = 2\partial^{2\alpha}_{x,a}\ln f(x, y, t), \tag{17}$$

*then fractional KP Equation (3) has the following bilinear form:*

$$\left(H^\alpha_{t,c}H^\alpha_{x,a} + H^{4\alpha}_{x,a} + 3\sigma H^{2\alpha}_{y,b}\right)f \cdot f = 0, \tag{18}$$

*where* $H^{\alpha}_{x,a}$, $H^{\alpha}_{y,b}$, *and* $H^{\alpha}_{t,c}$ *are the fractional versions [28] of the Hirota bilinear operator [5]:*

$$H^{m\alpha}_{x,a}H^{n\alpha}_{t,c}f\cdot g=\left(\partial^{\alpha}_{x,a}-\partial^{\alpha}_{x',a}\right)^{m}\left(\partial^{\alpha}_{t,c}-\partial^{\alpha}_{t',c}\right)^{n}f(x,t)g\cdot\left(x',t'\right)\Big|_{x'=x,t'=t},\ (m,n\in N). \tag{19}$$

*Proof.* Substituting Equation (17) into fractional KP Equation (3), we convert Equation (3) into

$$\partial^{\alpha}_{t,c}\left(\partial^{\alpha}_{x,a}f\right)-\left(\partial^{\alpha}_{t,c}f\right)\partial^{\alpha}_{x,a}f+f\left(\partial^{4\alpha}_{x,a}f\right)-4\left(\partial^{\alpha}_{x,a}f\right)\partial^{3\alpha}_{x,a}f+3\left(\partial^{2\alpha}_{x,a}f\right)^{2}+3\sigma\left(f\left(\partial^{2\alpha}_{y,b}f\right)-\left(\partial^{\alpha}_{y,b}f\right)^{2}\right)=0, \tag{20}$$

which can be rewritten as Equation (18) by using the fractional Hirota's bilinear operator (19). The proof ends.

With the help of the fractional bilinear form (18), we then obtain fractional $n$-soliton solutions of fractional KP Equation (3) as follows:

$$u=2\partial^{2\alpha}_{x,a}\ln\left(\sum_{\mu=0,1}e^{\sum_{j=1}^{n}\mu_j\xi_j+\sum_{1\le j<l}^{n}\mu_j\mu_1A_{jl}}\right), \tag{21}$$

where $\Sigma_{\mu=0,1}$ denotes all the possible combinations of each $\mu_j=\{0,1\}$ for $j=1,2,\cdots,n$,

$$\xi_j=k_j\left[\frac{(x-a)^{\alpha}}{\alpha}+p_j\frac{(y-b)^{\alpha}}{\alpha}-\left(k_j^2+3\sigma p_j^2\right)\frac{(t-c)^{\alpha}}{\alpha}\right]+\xi_j^{(0)}, \tag{22}$$

while $e^{A_{jl}}=[(k_j-k_l)^2-\sigma(p_j-p_l)^2]/[(k_j+k_l)^2-\sigma(p_j-p_l)^2]$, $k_j$, $p_j$, and $\xi_j^{(0)}$ are constants.

In particular, when $n=1$, Equation (21) gives the fractional one-soliton solution of fractional KP Equation (3):

$$u=2\partial^{2\alpha}_{x,a}\ln\left(1+e^{\xi_1}\right)=\frac{k_1^2}{2}\sec h^2\frac{\xi_1}{2}, \tag{23}$$

with

$$\xi_1=k_1\left[\frac{(x-a)^{\alpha}}{\alpha}+p_1\frac{(y-b)^{\alpha}}{\alpha}-\left(k_1^2+3\sigma p_1^2\right)\frac{(t-c)^{\alpha}}{\alpha}\right]+\xi_1^{(0)}. \tag{24}$$

Compared with one-soliton of integer order $\alpha=1$, we can see from Figures 1–6 that the fractional ones of the corresponding fractional KPII equation have different profiles. Figure 1 shows there are different wave widths. But the essential difference is that every fractional soliton has a certain inclination in the opposite direction of its propagation, as if it is affected by the resistance of the carrier in the forward direction. Such a characteristic also appears in Figure 2. More interestingly, the fractional one-soliton in Figure 2 has a bend in the middle; such phenomena often occur on the edges of flat beaches. In addition to the same amplitude $k_1^2/2$ and the similar bell profile known from Equation (23), to gain more insights in the dynamics of the one-solitons in Figure 1 mathematically, we insert $a=0$, $b=2$, $c=3$, $k_1=1$, $p_1=1/2$, $\sigma=1$, and $\xi_1^{(0)}=0$ into Equation (24); then, the velocity along the $x$-axis of the one-solitons can be derived by the expression

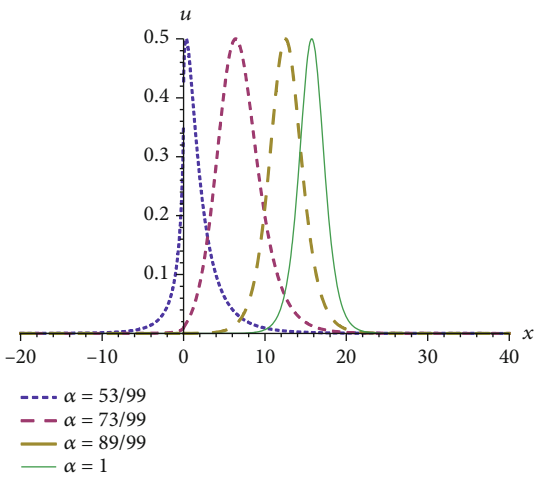


Figure 1: Profiles of fractional one-soliton $u$ with different orders by selecting $a=0$, $b=2$, $c=3$, $k_1=1$, $p_1=1/2$, $\sigma=1$, $\xi_1^{(0)}=0$, $y=-40$, and $t=0$.

$$\dot{x}=\frac{7}{4}(t-3)^{\alpha-1}\left[\frac{42^{\alpha}}{2}+\frac{7}{4}(t-3)^{\alpha}\right]^{1/\alpha-1}, \tag{25}$$

which shows that all the fractional one-solitons propagate along the $x$-axis with variable velocities depending on time $t$ and fractional order $\alpha$. However, the integral-order soliton propagates at a constant velocity of 7/4. At time $t=0$, the velocities corresponding to $\alpha=53/99, 73/99, 89/99$ are about 0.62, 2.14, and 2.02, respectively. The simulation results show that when $t=4$, all these fractional and integral-order solitons propagate to almost the same position along the positive direction of the $x$-axis, but when $t=8$, their positions in the positive direction of $x$-axis are just opposite to those when $t=0$. If $\dot{x}<0$, such as $t=-18$, all these solitons, whether integer or fractional, propagate along the negative $x$-axis, and when $t=-18$, they all reach the negative $x$-axis.

Figure 3 shows there are not only different wave widths but also amplitudes between the integer-order one-soliton and the fractional ones. Besides, a fractional one-soliton with $\alpha=53/98$ in Figure 4 appears two obvious wavelet peaks in

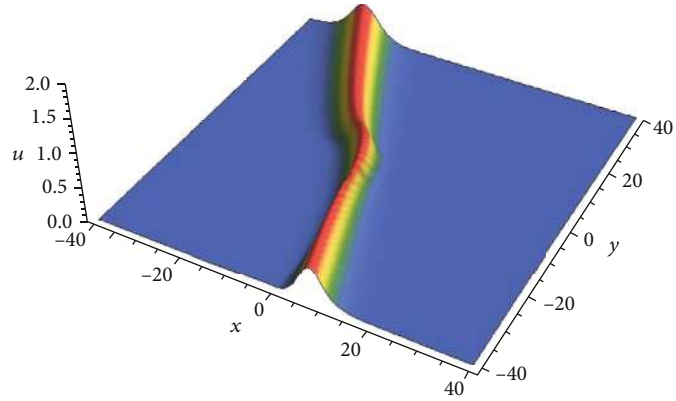


Figure 2: Fractional one-soliton $u$ with $\alpha = 73/99$ by selecting $a = 1$, $b = 2$, $c = 3$, $k_1 = 1$, $p_1 = 1/2$, $\sigma = 1$, $\xi_1^{(0)} = 0$, and $t = 0$.

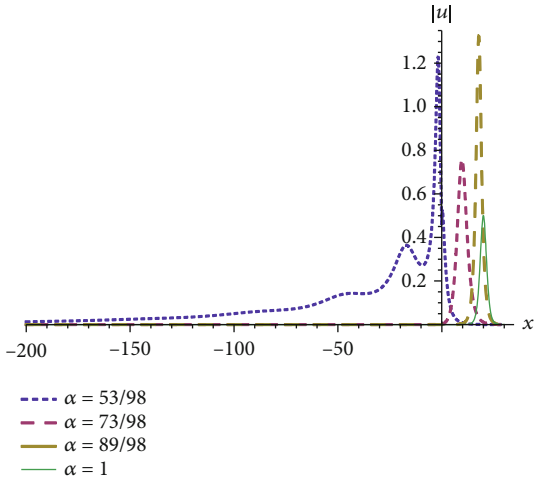


Figure 3: Profiles of fractional one-soliton $|u|$ with different orders by selecting $a = 1, b = 2, c = 3, k_1 = 1, p_1 = 1/2, \sigma = 1, \xi_1^{(0)} = 0, y = -40$, and $t = 0$.

the negative direction of $x$-axis. These different wave widths, amplitudes, and wavelet peaks in Figures 3 and 4 benefit from the fact that both $(x-a)^\alpha$ and $(y-b)^\alpha$ in Equation (24) return complex values according to Definition 1 for arbitrary $x < a$ and $y < b$ when $\alpha = p/q$ and $q$ is an even number. More specifically, it is known that $\sec h^2 z \le 4$ always holds for any $z \in R$, but it does not hold when $z = x + iy(x, y \neq 0 \in R)$ is a complex number. It is because that $|\text{sech } z|^2 = |1/(\cosh^2 x - \sin^2 y)|$ can reach any given positive number as long as $x$ and $y$ are selected appropriately. For example, $|\text{sech } (0.2 + 1.3i)|^2 > 8.9$.

Figures 5 and 6 indicate that the uplift in the middle of the fractional line one-solitons appears some features of peakons, the peaks of which have discontinuous first derivatives of integer order. For the fractional one-soliton $u$ with $\alpha = 6/11$, the limit of $u_x(x, y, t)$ at the point (1,1.5,0) is infinity. The reason that the peakons appear in Figures 5 and 6 is due to Definition 2 which let Equation (24) perform the computation $(x-a)^\alpha = [(x-a)^p]^{1/q}$ and $(y-b)^\alpha = [(y-b)^p]^{1/q}$ when $\alpha = p/q$ and $p$ is an even number.

*4.2. Fractional X-, Y-, and 3-in-2-out-Type Interactions.* Assign $n = 2$ to Equation (21), we first write the fractional two-soliton solution of fractional KP Equation (3) as

$$u = 2\partial_{x,a}^{2\alpha} \ln\left(1 + e^{\xi_1} + e^{\xi_2} + e^{\xi_1+\xi_2+A_{12}}\right), \tag{26}$$

where $\xi_1$ satisfies Equation (24), and

$$\xi_2 = k_2\left[\frac{(x-a)^\alpha}{\alpha} + p_2\frac{(y-b)^\alpha}{\alpha} - \left(k_2^2 + 3\sigma p_2^2\right)\frac{(t-c)^\alpha}{\alpha}\right] + \xi_2^{(0)},$$
$$e^{A_{12}} = \frac{(k_1-k_2)^2 - \sigma(p_1-p_2)^2}{(k_1+k_2)^2 - \sigma(p_1-p_2)^2}. \tag{27}$$

Next, we use the fractional two-soliton solution (26) to simulate the X- and Y-type interactions [1] observed by Abolwitz and Baldwin. Since the phase shifts of the colliding 2-solitons in a two-dimensional KdV equation are determined by $e^{A_{12}}$ in Equation (27), more details can be found in [29], we choose appropriate values of $e^{A_{12}}$ to simulate the X- and Y-type interactions through the fractional KPII equation. Based on the selection of $k_1 = 1/2$, $k_2 = 1/2$, $p_1 = 2/3$, $p_2 = -2/3$ [1], and $\sigma = 1$ letting $e^{A_{12}} \approx 2.3$, Figure 7 shows an X-type interaction formed by the fractional two-soliton solution (26) with $\alpha = 83/99$. At the same time, it should be noted that a phase shift caused by the collision of two-solitons will form the so-called "stem," so the change of $e^{A_{12}}$ will affect the length, height, and even disappearance of stem. By choosing $k_1 = 1/2$, $k_2 = 1$, $p_1 = 3/4$, $p_2 = 1$, and $\sigma = 1$ so that $e^{A_{12}} = 0$, Figure 8 simulates a Y-type interaction without a stem. In addition, two X-type interactions with long stem ($e^{A_{12}} \approx 5.0 \times 10^9$) and short stem ($e^{A_{12}} \approx 50.8$) are shown in Figures 9 and 10, respectively. In Figure 11, we show another X-type interaction, the stem corresponding to $e^{A_{12}} \approx 5.0 \times 10^{-8}$ of which is lower than one incoming line soliton not as the ones having high stems in Figures 7, 9, and 10, while is almost equal to the other incoming line soliton in height.

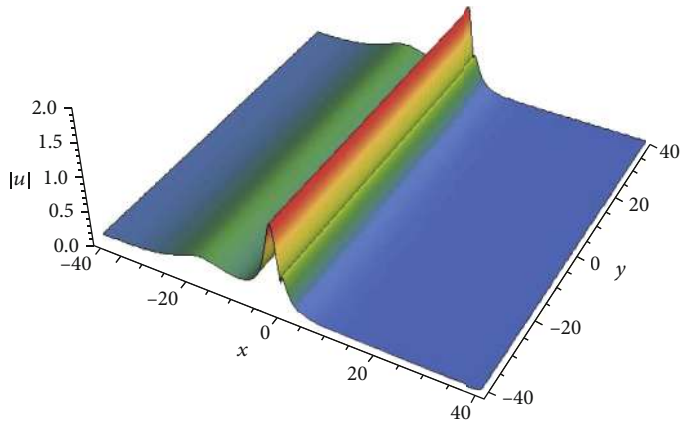


Figure 4: Fractional one-soliton $|u|$ with $\alpha = 53/98$ by selecting $a = 1$, $b = 1.5$, $c = 0$, $k_1 = 1$, $p_1 = 1/2$, $\sigma = 1$, $\xi_1^{(0)} = 0$, and $t = 0$.

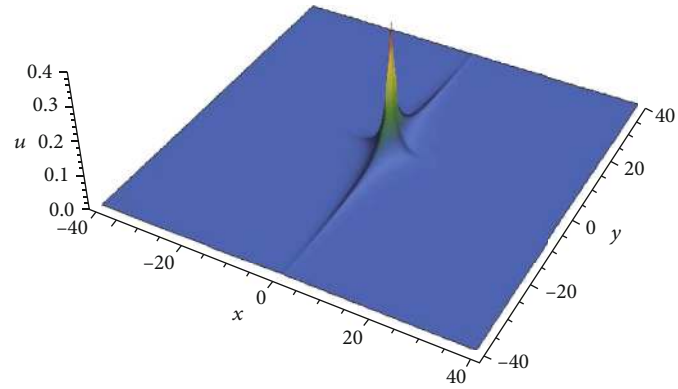


Figure 5: Peakon formed by the fractional one-soliton $u$ with $\alpha = 6/11$ by selecting $a = 1$, $b = 1.5$, $c = 0$, $k_1 = 1$, $p_1 = 1/2$, $\sigma = 1$, $\xi_1^{(0)} = 0$, and $t = 0$.

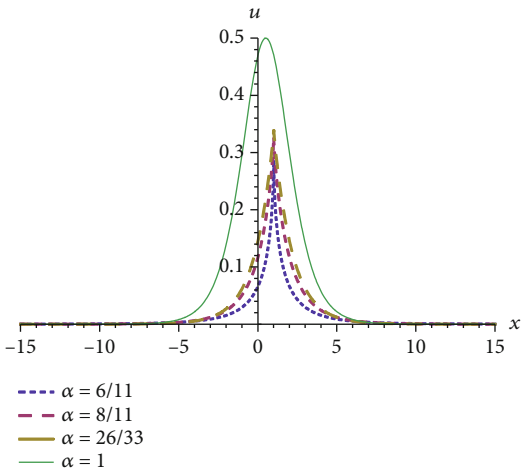


Figure 6: Profiles of fractional one-soliton $u$ with different orders by selecting $a = 1$, $b = 1.5$, $c = 0$, $k_1 = 1$, $p_1 = 1/2$, $\sigma = 1$, $\xi_1^{(0)} = 0$, $y = -1$, and $t = 0$.

Finally, we employ the fractional three-soliton solution of fractional KP Equation (3) to simulate not only X- and Y-type interactions but also 3-in-2-out-type interaction [1]. For this purpose, we write the fractional three-soliton solution by the substitution of $n = 3$ into Equation (21):

$$u = 2\partial_{x,a}^{2\alpha} \ln\left(1 + e^{\xi_1} + e^{\xi_2} + e^{\xi_3} + e^{\xi_1+\xi_2+A_{12}} + e^{\xi_1+\xi_3+A_{13}} + e^{\xi_2+\xi_3+A_{23}} + e^{\xi_1+\xi_2+\xi_3+A_{12}+A_{13}+A_{23}}\right), \tag{28}$$

where $\xi_1$ satisfies Equation (24), $e^{A_{12}}$ and $\xi_2$ are determined by Equation (27), and

$$\xi_3 = k_3\left[\frac{(x-a)^\alpha}{\alpha} + p_3\frac{(y-b)^\alpha}{\alpha} - \left(k_2^2 + 3\sigma p_3^2\right)\frac{(t-c)^\alpha}{\alpha}\right] + \xi_3^{(0)}, \tag{29}$$

$$e^{A_{13}} = \frac{(k_1-k_3)^2 - \sigma(p_1-p_3)^2}{(k_1+k_3)^2 - \sigma(p_1-p_3)^2},$$
$$e^{A_{23}} = \frac{(k_2-k_3)^2 - \sigma^2(p_2-p_3)^2}{(k_2+k_3)^2 - \sigma(p_2-p_3)^2}. \tag{30}$$

Substituting $k_1 = 0.2$, $k_2 = 1.2$, $k_3 = 2.2$, $p_1 = -1/4$, $p_2 = -3/4$, $p_3 = -7/4$, and $\sigma = 1$ into Equations (24) and (27), we

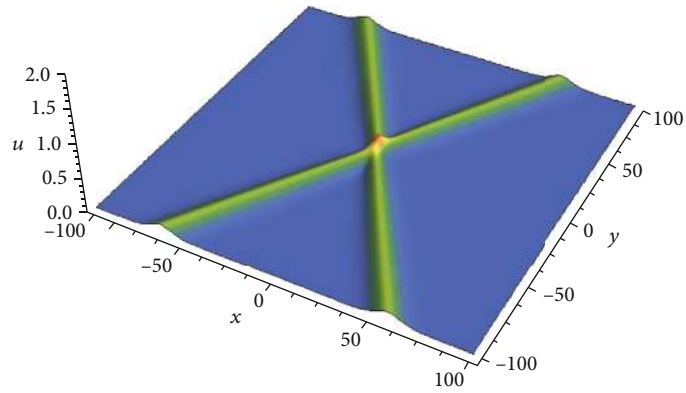


Figure 7: X-type interaction in the fractional line two-soliton solution $u$ with $\alpha = 83/99$, $a = 0$, $b = 0$, $c = 0$, $k_1 = 1/2$, $k_2 = 1/2$, $p_1 = 2/3$, $p_2 = -2/3$, $\sigma = 1$, $\xi_1^{(0)} = 0$, and $\xi_2^{(0)} = 0$.

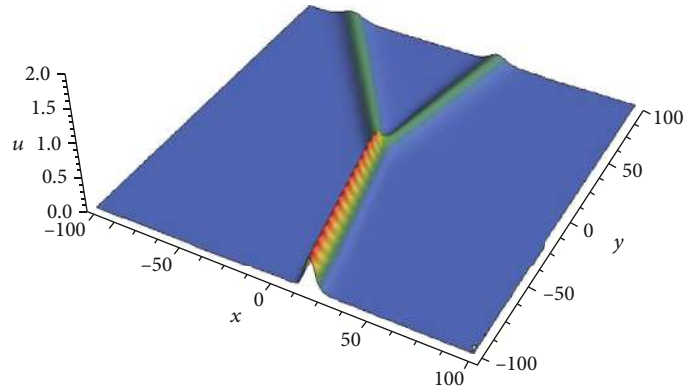


Figure 8: Y-type interaction in the fractional line two-soliton solution $u$ with $\alpha = 83/99$, $a = 0$, $b = 0$, $c = 0$, $k_1 = 1/2$, $k_2 = 1$, $p_1 = 3/4$, $p_2 = 1$, $\sigma = 1$, $\xi_1^{(0)} = 0$, and $\xi_2^{(0)} = 0$.

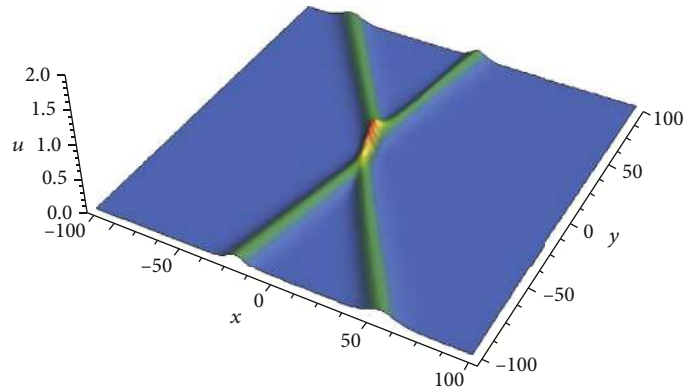


Figure 9: X-type interaction with a short stem in the fractional line two-soliton solution $u$ with $\alpha = 83/99$, $a = 0$, $b = 0$, $c = 0$, $k_1 = 1/2$, $k_2 = 1/2$, $p_1 = -1/4 - 10^{-2}$, $p_2 = 3/4$, $\sigma = 1$, $\xi_1^{(0)} = 0$, and $\xi_2^{(0)} = 0$.

have $e^{A_{12}} \approx 0.4$, $e^{A_{13}} \approx 0.5$, and $e^{A_{23}} \approx 4.2 \times 10^{-17}$; then, an X-type interaction forming in the fractional line three-soliton solution (28) with $\alpha = 83/99$ is shown in Figure 12. Interestingly, the remarkable differences from Figure 11 are the stem in Figure 12 which is lower than all the two incoming line solitons and one curved outgoing line soliton. The appropriate parameters $k_1$, $k_2$, and $k_3$, which are only slightly different from those in Figure 12, are selected; Figure 13 shows a Y-type structure ($e^{A_{12}} \approx 0.56$, $e^{A_{13}} \approx 0.61$, $e^{A_{23}} = 0$) in the same fractional line three-soliton solution (28). In Figure 14, we show a 3-in-2 out-type interaction, one line soliton of which has high amplitude than all the incoming ones, where $e^{A_{12}} \approx 0.08$, $e^{A_{13}} \approx 0.12$, and $e^{A_{23}} = 0$ are determined by selecting $k_1 = 1$, $k_2 = 2$, $k_3 = 2$, $p_1 = -1/3$, $p_2 = -2/3$, $p_3 = -5/3$, and $\sigma = 1$.

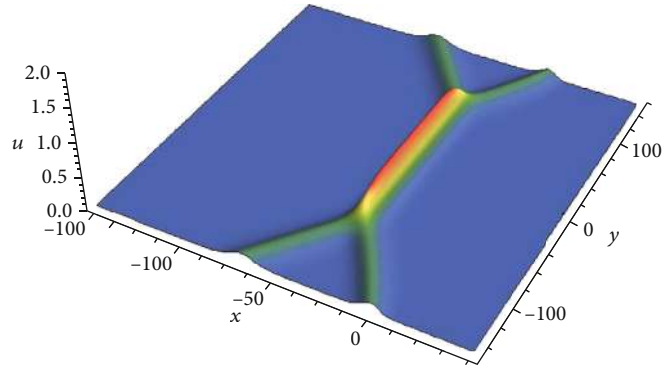


Figure 10: X-type interaction with a long stem in the fractional line two-soliton solution $u$ with $\alpha = 83/99$, $a = 0$, $b = 0$, $c = 0$, $k_1 = 1/2$, $k_2 = 1/2$, $p_1 = -1/2 - 10^{-10}$, $p_2 = 1/2$, $\sigma = 1$, $\xi_1^{(0)} = 0$, and $\xi_2^{(0)} = 0$.

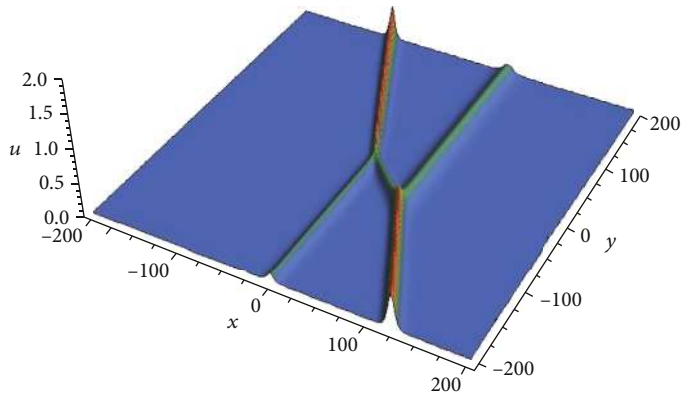


Figure 11: X-type interaction with a low stem in the fractional line two-soliton solution $u$ with $\alpha = 83/99$, $a = 0$, $b = 0$, $c = 0$, $k_1 = 1$, $k_2 = 1/2$, $p_1 = 1/2 - 10^{-7}$, $p_2 = 0$, $\sigma = 1$, $\xi_1^{(0)} = 0$, and $\xi_2^{(0)} = 0$.

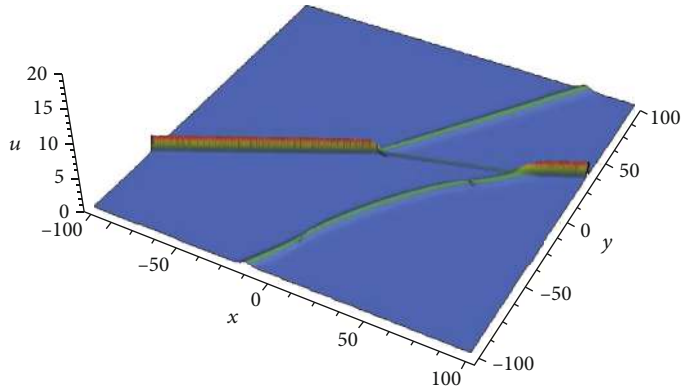


Figure 12: X-type interaction in the fractional line three-soliton solution $u$ with $\alpha = 83/99$, $a = 0$, $b = 0$, $c = 0$, $k_1 = 0.2$, $k_2 = 1.2$, $k_3 = 2.2$, $p_1 = -1/4$, $p_2 = -3/4$, $p_3 = -7/4$, $\sigma = 1$, $\xi_1^{(0)} = 0$, $\xi_2^{(0)} = 0$, and $\xi_3^{(0)} = 0$.

*4.3. Falling and Spreading Phenomena of a Columnar Structure.* As mentioned earlier, all the values of $e^{A_{12}}$, $e^{A_{13}}$, and $e^{A_{23}}$ in Figures 7–14 are nonnegative. From the forms of their compositions in Equations (27) and (30), we can see that $e^{A_{12}}$, $e^{A_{13}}$, and $e^{A_{23}}$ can also take negative values. In Figures 15(a)–15(l), we show a falling and spreading process of a columnar structure ($e^{A_{12}} \approx -0.3$) in the fractional two-soliton solution (26) of the fractional KPII equation, where the parameters are selected as $\alpha = 82/99$, a = 0, $b = 0$, $c = 0$, $k_1 = -1/2$, $k_2 = -1/2$, $p_1 = 1/4 - 10^{-4}$, $p_2 = 4/3$, $\sigma = 1$, $\xi_1^{(0)} = 0$, and $\xi_2^{(0)} = 0$, respectively. In this case, for any fixed time $t$, the limit of the amplitude $u$ of this fractional two-soliton always tends to zero as $x \longrightarrow \pm\infty$ and $y \longrightarrow \pm\infty$. Figure 15(a) shows the columnar structure at the beginning $t = 0$. With the passage of time, the top of the columnar began to fall vertically, forming a column in the opposite

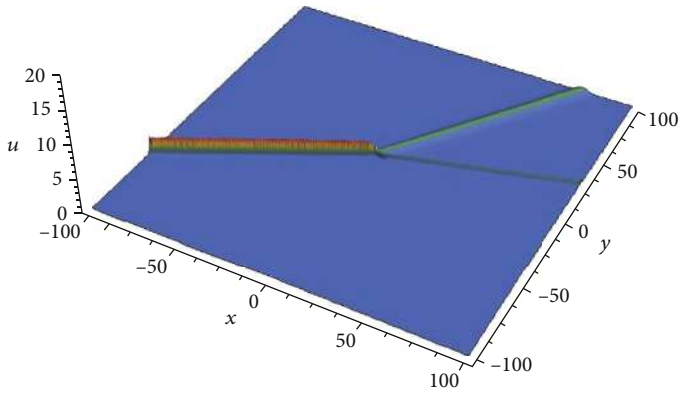


Figure 13: Y-type interaction in the fractional line three-soliton solution $u$ with $\alpha = 83/99$, $a = 0$, $b = 0$, $c = 0$, $k_1 = 0.13$, $k_2 = 1.13$, $k_3 = 2.13$, $p_1 = -1/4$, $p_2 = -3/4$, $p_3 = -7/4$, $\sigma = 1$, $\xi_1^{(0)} = 0$, $\xi_2^{(0)} = 0$, and $\xi_3^{(0)} = 0$.

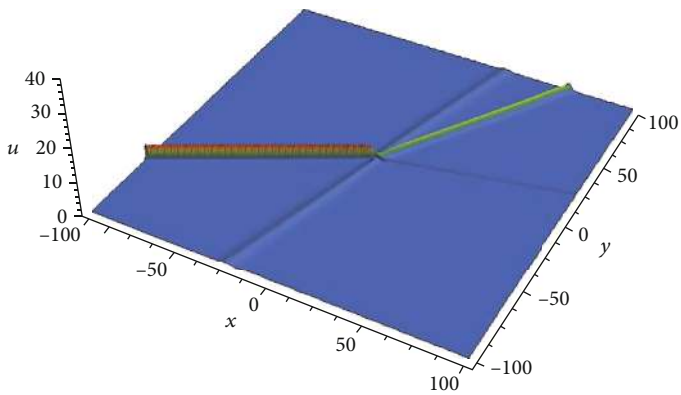


Figure 14: 3-in-2-out-type interaction in the fractional line three-soliton solution $u$ with $\alpha = 83/99$, $a = 0$, $b = 0$, $c = 0$, $k_1 = 1$, $k_2 = 2$, $k_3 = 2$, $p_1 = -1/3$, $p_2 = -2/3$, $p_3 = -5/3$, $\sigma = 1$, $\xi_1^{(0)} = 0$, $\xi_2^{(0)} = 0$, and $\xi_3^{(0)} = 0$.

direction and widening continuously, until at $t = 18.83$ the column suddenly shrinks into a very thin inverted cone, see Figures 15(b)–15(g). Then, the inverted cone becomes slender and splits into several inverted cones from about $t = 19.2$. When $t = 20.5$, the number of inverted cones began to decrease, and diamond pattern was formed on the background, see Figures 15(h) and 15(i). Finally, the number of inverted cones increases gradually, and the diamond background pattern gradually expands, see Figures 15(j)–15(l). In time inversion, the process of falling and spreading simulated in Figures 15 forms a long flat column, and the merging effect, as pointed out by Ablowitz and Baldwin [1], produced by multiple such columns may be useful to explain the generation of tsunami caused by earthquake.

*4.4. Fractional Rational Solution and Lump Structure.* Expanding Equation (18) yields

$$f_{x,a;t,c}^{(2\alpha)} f - f_{x,a}^{(\alpha)} f_{t,c}^{(\alpha)} + f_{x,a}^{(4\alpha)} f - 4 f_{x,a}^{(3\alpha)} f_{x,a}^{(\alpha)} + 3\left(f_{x,a}^{(2\alpha)}\right)^2 + 3\sigma\left(f_{y,b}^{(2\alpha)} f - \left(f_{y,b}^{(2\alpha)}\right)^2\right) = 0. \tag{31}$$

Following Ma's work [4], we suppose that

$$f = g^2 + h^2 + a_9, \tag{32}$$

with

$$g = a_1(x-a)^\alpha + a_2(y-b)^\alpha + a_3(t-c)^\alpha + a_4, \tag{33}$$

$$h = a_5(x-a)^\alpha + a_6(y-b)^\alpha + a_7(t-c)^\alpha + a_8, \tag{34}$$

where $a_i (i = 1, 2, \cdots, 9)$ are undetermined constants. Substituting Equations (32)–(34) into Equation (31), collecting the coefficients of the same powers $[(x-a)^\alpha]^j [(y-b)^\alpha]^l [(t-c)^\alpha]^s (j, l, s = 0, 1, 2, \cdots)$, we derive a set of algebraic equations about these undermined constants. Solving this set of algebraic equations, we can determine Equations (32)–(34) by

$$a_3 = -\frac{3\sigma\left[2a_2a_5a_6 + a_1\left(a_2^2 - a_6^2\right)\right]}{a_1^2 + a_5^2}, \tag{35}$$

$$a_7 = -\frac{3\sigma\left(-a_2^2a_5 + 2a_1a_2a_6 + a_5a_6^2\right)}{a1^2 + a5^2}, \qquad a_9 = -\frac{\left(a_1^2 + a_5^2\right)^3\alpha^2}{\sigma\left(a_2a_5 - a_1a_6\right)^2}. \tag{36}$$

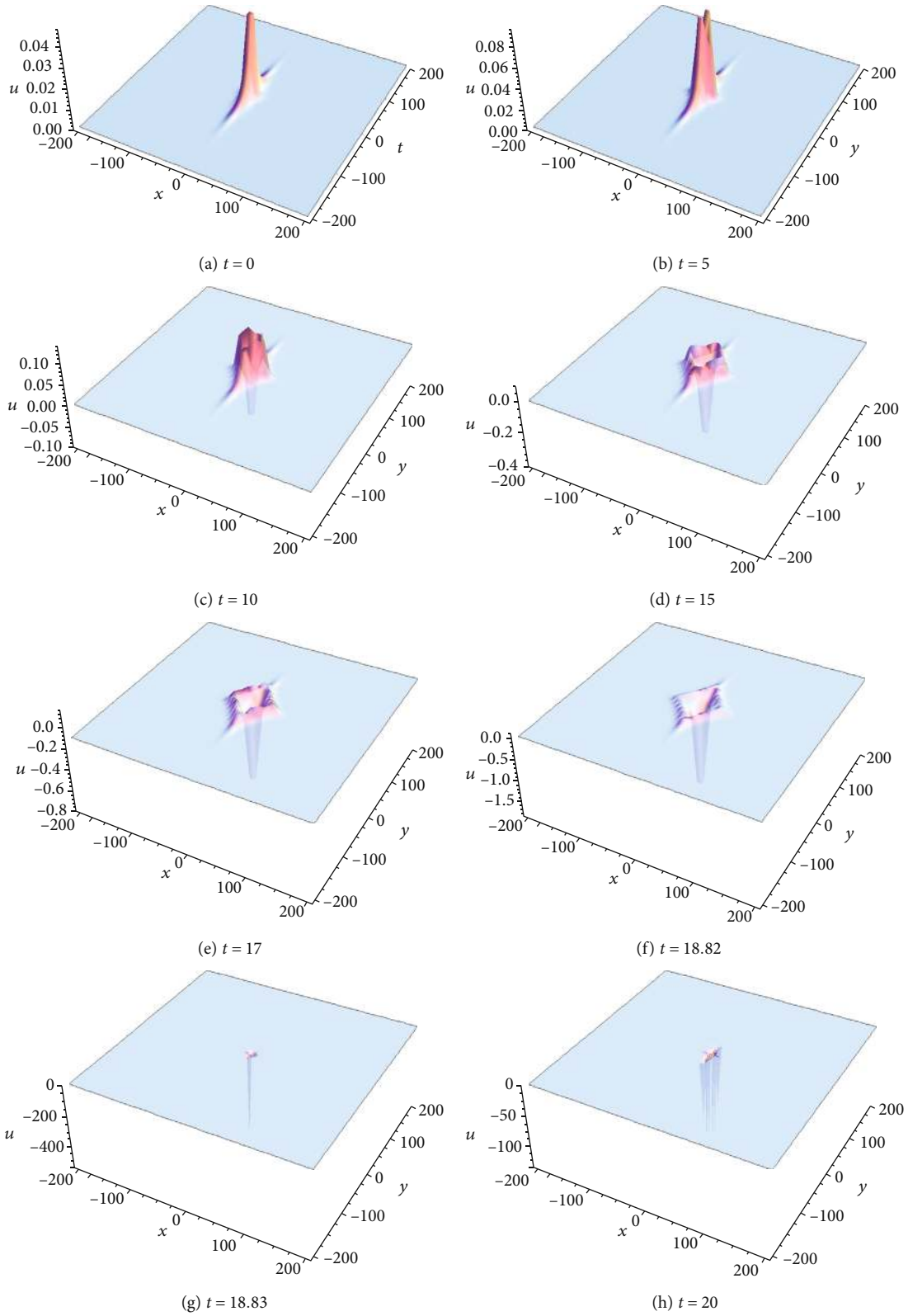


(a) $t = 0$ (b) $t = 5$

(c) $t = 10$ (d) $t = 15$

(e) $t = 17$ (f) $t = 18.82$

(g) $t = 18.83$ (h) $t = 20$

Figure 15: Continued.

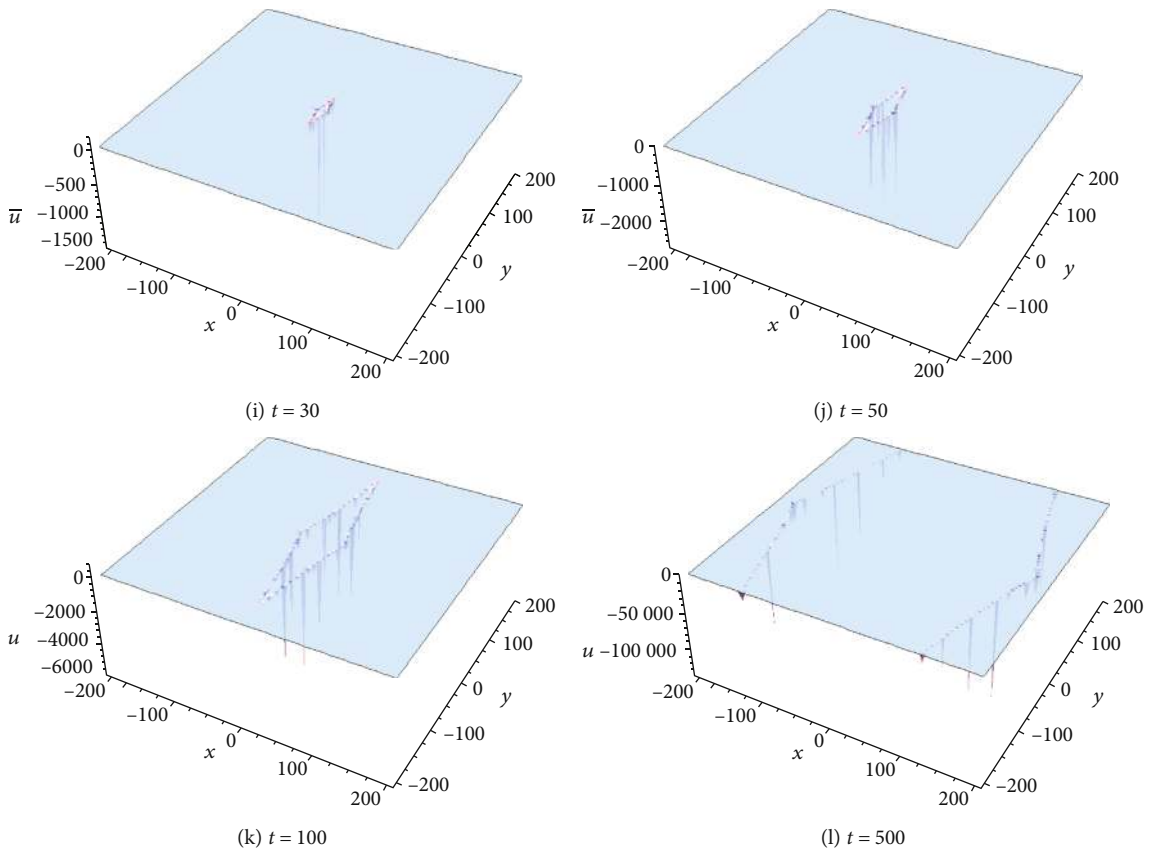


Figure 15: Falling and spreading phenomena of a columnar structure in the fractional two-soliton solution $u$ with $\alpha = 82/99$.

In view of Equations (17) and (32)–(36), we obtain a rational solution of fractional KP Equation (3):

$$u = 4\alpha^2 \frac{-\left[(x-a)^\alpha + a_2(y-b)^\alpha + 3\left(a_2^2 - a_6^2\right)(t-c)^\alpha + a_4^2\right]^2 + \left[a_6(y-b)^\alpha + 6a_2a_6(t-c)^\alpha + a_8^2\right]^2 - \left(\alpha^2/a_6^2\sigma\right)}{\left\{\left[(x-a)^\alpha + a_2(y-b)^\alpha + 3\left(a_2^2 - a_6^2\right)(t-c)^\alpha\right]^2 + \left[a_6(y-b)^\alpha + 6a_2a_6(t-c)^\alpha\right]^2 - \left(\alpha^2/a_6^2\sigma\right)\right\}^2} \tag{37}$$

by setting $a_1 = 1$ and $a_5 = 0$. Further inserting $a_4 = 0$, $a_8 = 0$, and $\sigma = -1$ into Equation (37), we reduce Equation (37) to a fractional lump solution of the fractional KPI equation:

$$u = 4\alpha^2 \frac{-\left[(x-a)^\alpha + a_2(y-b)^\alpha + 3\left(a_2^2 - a_6^2\right)(t-c)^\alpha\right]^2 + \left[a_6(y-b)^\alpha + 6a_2a_6(t-c)^\alpha\right]^2 + \left(\alpha^2/a_6^2\right)}{\left\{\left[(x-a)^\alpha + a_2(y-b)^\alpha + 3\left(a_2^2 - a_6^2\right)(t-c)^\alpha\right]^2 + \left[a_6(y-b)^\alpha + 6a_2a_6(t-c)^\alpha\right]^2 + \left(\alpha^2/a_6^2\right)\right\}^2}. \tag{38}$$

In Figure 16, the fractional lump solution (38) with $\alpha = 91/99$ of the fractional KPI equation is shown by setting $a = 0.5$, $b = 0.1$, $c = -0.3$, $a_2 = -0.2$, $a_6 = 1.2$, and $t = 0$. Here, we note that no matter whether $x - a$ and $y - b$ in Equation (38) are nonnegative or not, when $\alpha = p/q$ and $q$ is a odd number, Definition 1 always returns a unique real number from $(x-a)^\alpha$ and $(y-b)^\alpha$, respectively. Therefore, when we choose other different values of $a$ and $b$, the solution (38) can still maintain such lump structure in the space coordinate plane; only the positions are different. In the next subsection, we will simulate different spatial evolution structures presented by solution (38) in different positions of the coordinate plane.

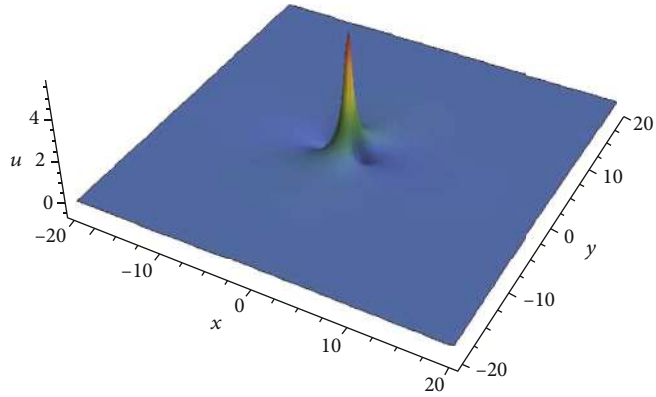


Figure 16: Fractional lump solution $|u|$ with $\alpha = 91/99$ and $a = 0.5$, $b = 0.1$, $c = -0.3$, $a_2 = -0.2$, $a_6 = 1.2$, and $t = 0$.

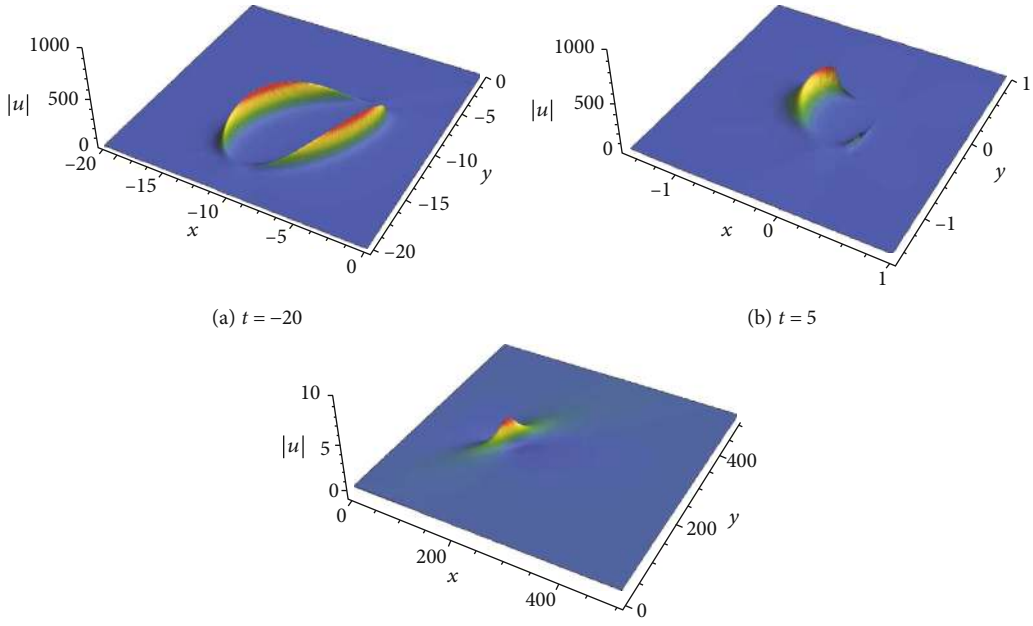


(a) $t = -20$ (b) $t = 5$

(c) $t = 20$

Figure 17: Dynamic evolution of the fractional lump solution $|u|$ with $\alpha = 51/98$, $a = 0.2$, $b = 0$, $c = 0$, $a_2 = -0.6$, and $a_6 = 0.8$.

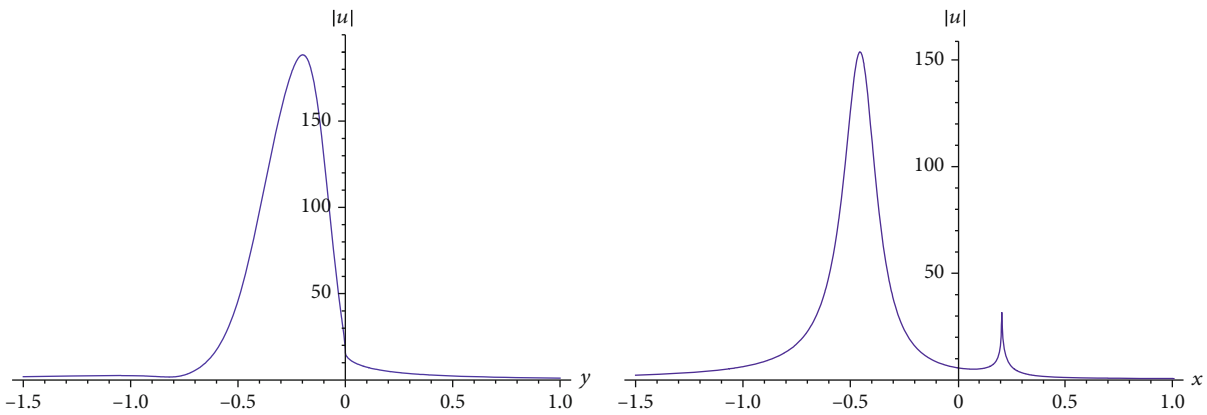


(a) $x = -0.5$ (b) $y = -0.35$

Figure 18: Profiles of the fractional lump solution $|u|$ with $\alpha = 51/98$, $a = 0.2$, $b = 0$, $c = 0$, $a_2 = -0.6$, $a_6 = 0.8$, and $t = 0$.

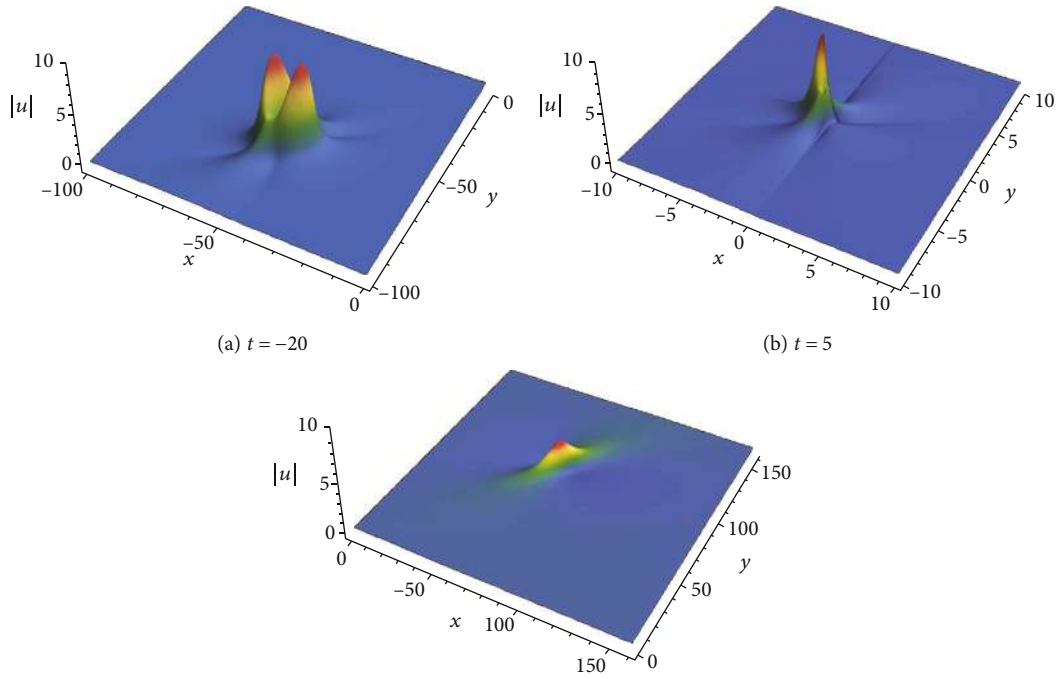


(a) $t = -20$ (b) $t = 5$

(c) $t = 20$

FIGURE 19: Dynamic evolution of the fractional lump solution $|u|$ with $\alpha = 61/98$, $a = 0.2$, $b = 0$, $c = 0$, $a_2 = -0.6$, and $a_6 = 0.8$.

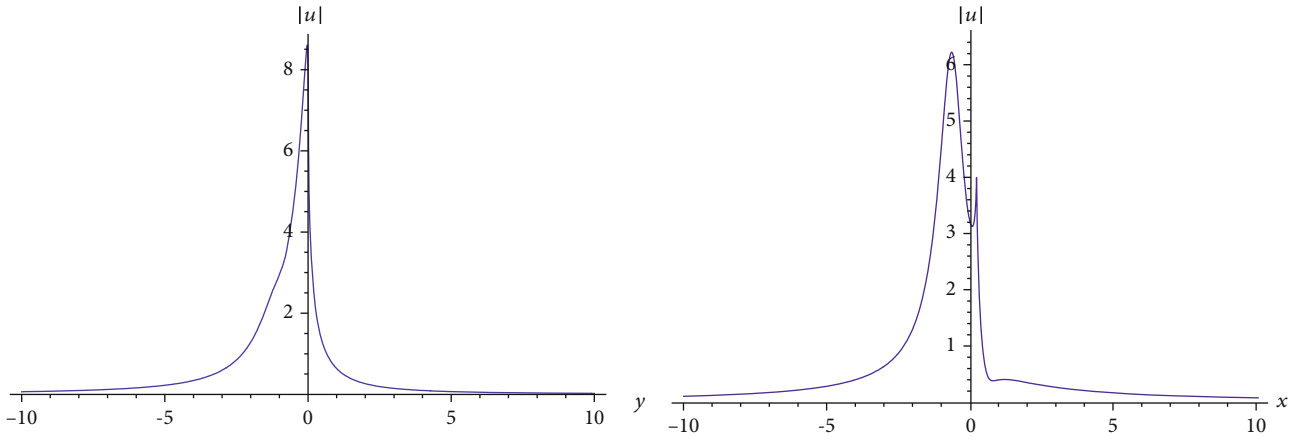


(a) $x = -0.5$ (b) $y = -0.35$

FIGURE 20: Profiles of the fractional lump solution $|u|$ with $\alpha = 61/98$, $a = 0.2$, $b = 0$, $c = 0$, $a_2 = -0.6$, $a_6 = 0.8$, and $t = 0$.

*4.5. Dynamic Evolutions from Ring and Conical Structures to Lump Structure.* In order to simulate the different spatial evolution structures of solution (38) in the same evolution process, we pay attention to the positive and negative effects of $x - a$, $y - b$, and $t - c$, so that $(x - a)^{\alpha}$, $(y - b)^{\alpha}$, and $(t - c)^{\alpha}$ are real numbers in a certain range and complex numbers in other ranges, see Figures 17–20 for examples. Figure 17 shows the dynamic evolution of the fractional lump solution (38) by the selection of $\alpha = 51/98$, $a = 0.2$, $b = 0$, $c = 0$, $a_2 = -0.6$, and $a_6 = 0.8$, where the spatial structure of $|u|$ changes from ring to lump. Two profiles of the fractional lump solution (38) at time $t = 0$ are shown in Figure 18. With a different fractional order $\alpha = 61/98$, Figure 19 shows another dynamic evolution of the fractional lump solution (38), where the spatial structure of $|u|$ changes from cone to lump. Two different profiles of the fractional lump solution (38) at time $t = 0$ are shown in Figure 20.

## 5. Conclusions

Based on the definitions of the conformable fractional partial derivatives and integrals, fractional KP Equation (3) with Lax integrability is derived. Then, a formula (21) of the fractional $n$-soliton solutions and rational solution (37) of KP Equation (3) is obtained by employing the Hirota bilinear method with fractional bilinear operators. When the fractional order $\alpha = 1$,

most of the simulated fractional X-, Y-, and 3-in-2-out-type interactions and fractional lump structures deform to the ones which can be constructed in [1, 4]. Even though, the selectivity of fractional order $\alpha$ results in the variation of velocity of soliton evolution propagation, the nonlinearity of motion trajectory, the inclination and steepness of appearance profile, the changeability of amplitude, the bend and wavelet peaks as well as peakon in the fractional line one-soliton, the falling and spreading process of a columnar structure in the fractional line two-soliton, and the ring and conical structures before lump structure generation are novel. This is due to the fractional partial derivatives contained in the fractional KP equation, which make the fractional soliton and lump solutions show different nonlinearity at different positions in the coordinate plane. In order to better understand the conformable fractional derivatives and integrals, this paper also attempts to give a physical explanation of the conformable fractional derivative from the perspective of variable acceleration. Extending fractional calculus to other important topics of nonlinear integrable systems is worth studying, such as soliton molecules [30], full reversal symmetric multiple soliton solutions [31], financial rogue wave [32], long-time asymptotic behavior [33], initial-boundary value problems [34], and high-dimensional hierarchies of evolution equations and their Hamiltonian structures [35].

## Data Availability

The data in the manuscript are available from the corresponding authors upon reasonable request.

## Conflicts of Interest

The authors declare that there is no conflict of interest regarding the publication of this article.

## Acknowledgments

This research was supported by the National Science Foundation of China (11971475), the Liaoning BaiQianWan Talents Program of China (2019), the Natural Science Foundation of Education Department of Liaoning Province of China (LJ2020002), and the Natural Science Foundation of Xinjiang Autonomous Region of China (2020D01B01).

## References

[1] M. J. Ablowitz and D. E. Baldwin, "Nonlinear shallow ocean-wave soliton interactions on flat beaches," *Physical Review E*, vol. 86, no. 3, article 036305, 2012.

[2] B. B. Kadomtsev and V. I. Petviashvili, "On the stability of solitary waves in weakly dispersing media," *Soviet Physics Doklady*, vol. 15, pp. 539–541, 1970.

[3] D. J. Korteweg and G. de Vries, "On the change of form of long waves advancing in a rectangular canal, and on a new type of long stationary," *Philosophical Magazine Series 5*, vol. 39, pp. 422–443, 1895.

[4] W. X. Ma, "Lump solutions to the Kadomtsev-Petviashvili equation," *Physics Letters A*, vol. 379, no. 36, pp. 1975–1978, 2015.

[5] R. Hirota, "Exact solution of the Korteweg-de Vries equation for multiple collisions of solitons," *Physical Review Letters*, vol. 27, no. 18, pp. 1192–1194, 1971.

[6] K. M. Kolwankar and A. D. Gangal, "Fractional differentiability of nowhere differentiable functions and dimensions," *Chaos*, vol. 6, no. 4, pp. 505–513, 1996.

[7] I. Podlubny, *Fractional Differential Equations: An Introduction to Fractional Derivatives, Fractional Differential Equations to Methods of Their Solution and Some of Their Applications*, Academic Press, New York, 1998.

[8] D. Brockmann, L. Hufnagel, and T. Geisel, "The scaling laws of human travel," *Nature*, vol. 439, no. 7075, pp. 462–465, 2006.

[9] J. Fujioka, A. Espinosa, and R. F. Rodríguez, "Fractional optical solitons," *Physics Letters A*, vol. 374, no. 9, pp. 1126–1134, 2010.

[10] J. H. He, "A tutorial review on fractal spacetime and fractional calculus," *International Journal of Theoretical Physics*, vol. 53, no. 11, pp. 3698–3718, 2014.

[11] X. J. Yang, D. Baleanu, and H. M. Srivastava, *Local Fractional Integral Transforms and Their Applications*, Academic Press, London, 2015.

[12] C. Cattani, H. M. Srivastava, and X. J. Yang, *Fractional Dynamics*, De Gruyter, Warsaw, 2015.

[13] S. Zhang, B. Cai, and B. Xu, "Variable separation method for nonlinear time fractional biological population model," *International Journal of Numerical Methods for Heat and Fluid Flow*, vol. 25, no. 7, pp. 1531–1541, 2015.

[14] Y. Hu and J. H. He, "On fractal space-time and fractional calculus," *Thermal Science*, vol. 20, no. 3, pp. 773–777, 2016.

[15] M. A. Abdou, S. Owyed, S. S. Ray, Y. M. Chu, M. Inc, and L. Ouahid, "Fractal ion acoustic waves of the space-time fractional three dimensional KP equation," *Advances in Mathematical Physics*, vol. 2020, Article ID 8323148, 7 pages, 2020.

[16] Q. Wang, X. Shi, J. H. He, and Z. B. Li, "Fractal calculus and its application to explanation of biomechanism of polar bear hairs," *Fractals*, vol. 26, no. 6, article 1850086, 2019.

[17] J. H. He, "Fractal calculus and its geometrical explanation," *Results in Physics*, vol. 10, pp. 272–276, 2018.

[18] Y. Wang and Q. Deng, "Fractal derivative model for tsunami traveling," *Fractals*, vol. 27, no. 2, article 1950017, 2019.

[19] J. H. He and F. Y. Ji, "Two-scale mathematics and fractional calculus for thermodynamics," *Thermal Science*, vol. 23, no. 4, pp. 2131–2133, 2019.

[20] J. Fan and X. M. Shang, "Fractal heat transfer in wool fiber hierarchy," *Heat Transfer Research*, vol. 44, no. 5, pp. 399–407, 2013.

[21] J. Fan, N. Zhu, L. L. Wang, Z. Liu, C. Y. Wang, and Y. Liu, "Influence of hierarchic structure on the moisture permeability of biomimic woven fabric using fractal derivative method," *Advances in Mathematical Physics*, vol. 2015, Article ID 817437, 4 pages, 2015.

[22] M. Bagheri and A. Khani, "Analytical method for solving the fractional order generalized KdV equation by a beta-fractional derivative," *Advances in Mathematical Physics*, vol. 2020, Article ID 8819183, 18 pages, 2020.

[23] D. Shi and Y. Zhang, "Diversity of exact solutions to the conformable space-time fractional MEW equation," *Applied Mathematics Letters*, vol. 99, article 105994, 2020.

[24] T. Abdeljawad, "On conformable fractional calculus," *Journal of Computational and Applied Mathematics*, vol. 279, pp. 57–66, 2015.

[25] R. Khalil, M. al Horani, A. Yousef, and M. Sababheh, "A new definition of fractional derivative," *Journal of Computational and Applied Mathematics*, vol. 264, no. 5, pp. 65–70, 2014.

[26] D. Y. Xue, *Fractional Calculus and Fractional-Order Control*, Science Press, Beijing, 2018.

[27] Podlubny, "Geometric and physical interpretations of fractional integration and differentiation," *Fractional Calculus and Applied Analysis*, vol. 5, pp. 230–237, 2001.

[28] S. Zhang, Y. Wei, and B. Xu, "Bilinearization and fractional soliton dynamics of fractional Kadomtsev-Petviashvili equation," *Thermal Science*, vol. 23, 3 Part A, pp. 1425–1431, 2019.

[29] J. Satsuma, "$N$-soliton solution of the two-dimensional Korteweg-deVries equation," *Journal of the Physical Society of Japan*, vol. 40, no. 1, pp. 286–290, 1976.

[30] S. X. Yang, Z. Zhang, and B. Li, "Soliton molecules and some novel types of hybrid solutions to $(2+1)$-dimensional variable-coefficient Caudrey-Dodd-Gibbon-Kotera-Sawada equation," *Advances in Mathematical Physics*, vol. 2020, Article ID 2670710, 9 pages, 2020.

[31] S. Y. Lou, "Full reversal symmetric multiple soliton solutions for integrable systems," *Acta Physica Sinica*, vol. 69, no. 1, article 01053, 2020.

[32] Z. Y. Yan, "Financial rogue waves," *Communications in Theoretical Physics*, vol. 54, no. 5, pp. 947–949, 2010.

[33] J. Xu, E. Fan, and Y. Chen, "Long-time asymptotic for the derivative nonlinear Schrödinger equation with step-like initial value," *Mathematical Physics, Analysis and Geometry*, vol. 16, no. 3, pp. 253–288, 2013.

[34] S. F. Tian, "Initial-boundary value problems for the general coupled nonlinear Schrödinger equation on the interval via the Fokas method," *Journal of Differential Equations*, vol. 262, no. 1, pp. 506–558, 2017.

[35] Y. Zhang, J. Gao, and G. Wang, "Two $(2+1)$-dimensional hierarchies of evolution equations and their Hamiltonian structures," *Applied Mathematics and Computation*, vol. 243, pp. 601–606, 2014.